

# PCCP

Accepted Manuscript



This is an *Accepted Manuscript*, which has been through the Royal Society of Chemistry peer review process and has been accepted for publication.

*Accepted Manuscripts* are published online shortly after acceptance, before technical editing, formatting and proof reading. Using this free service, authors can make their results available to the community, in citable form, before we publish the edited article. We will replace this *Accepted Manuscript* with the edited and formatted *Advance Article* as soon as it is available.

You can find more information about *Accepted Manuscripts* in the [Information for Authors](#).

Please note that technical editing may introduce minor changes to the text and/or graphics, which may alter content. The journal's standard [Terms & Conditions](#) and the [Ethical guidelines](#) still apply. In no event shall the Royal Society of Chemistry be held responsible for any errors or omissions in this *Accepted Manuscript* or any consequences arising from the use of any information it contains.

**Facile Electrochemical Co-Deposition of a Graphene/Cobalt Nanocomposite for Highly Efficient Water Oxidation in Alkaline Media: Direct Detection of Underlying Electron Transfer Reactions Under Catalytic Turnover Conditions†**

Si-Xuan Guo,<sup>a</sup> Yuping Liu,<sup>a</sup> Alan M. Bond<sup>\*a</sup> and Jie Zhang<sup>\*a</sup>

Esakki Karthik,<sup>b</sup> Ilango Maheswaran,<sup>b</sup> Senthil Kumar<sup>b</sup> and Kanala L.N. Phani<sup>\*b</sup>

**Abstract:**

A facile electrochemical co-deposition method has been developed for the fabrication of graphene/cobalt nanocomposite modified electrodes that achieve highly efficient water oxidation in highly alkaline media. In the method reported, a graphene/cobalt nanocomposite film was deposited electrochemically from a medium containing  $1 \text{ mg ml}^{-1}$  graphene oxide,  $0.8 \text{ mM}$  cobalt nitrate and  $0.05 \text{ M}$  phytic acid (pH 7). The formation of the nanocomposite film was confirmed using electrochemical, Raman spectroscopic and scanning electron microscopic techniques. The nanocomposite film exhibits excellent activity and stability towards water oxidation to generate oxygen in  $1 \text{ M NaOH}$  aqueous electrolyte media. A turn over frequency of  $34 \text{ s}^{-1}$  at an overpotential of  $0.59 \text{ V}$  and a faradaic efficiency of  $97.7\%$  were deduced from analysis of data obtained by rotating ring disk electrode voltammetry. Controlled potential electrolysis data suggests that the graphene supported catalyst exhibits excellent stability under these harsh conditions. Phytate anion acts as stabilizer for the electrochemical formation of cobalt nanoparticles. Fourier transformed ac voltammetry allowed the redox chemistry associated with catalysis to be detected directly under catalytic turnover conditions. Estimates of formal reversible potentials obtained from this method for the reactions  $3 \text{ Co(OH)}_2 + 2 \text{ OH}^- \rightleftharpoons \text{Co}_3\text{O}_4 + 4 \text{ H}_2\text{O} + 2 \text{ e}^-$ ,  $\text{Co}_3\text{O}_4 + \text{ OH}^- \rightleftharpoons 3 \text{ CoOOH} + \text{ e}^-$  and  $\text{CoOOH} + \text{ OH}^- \rightleftharpoons \text{CoO}_2 + \text{ H}_2\text{O} + \text{ e}^-$  are  $0.10$ ,  $0.44$  and  $0.59 \text{ V}$  vs.  $\text{Ag/AgCl}$ , respectively.

**Introduction:**

Graphene is a carbon material with an ideal two-dimensional structure consisting of a sheet of carbon atoms, one-atom-thick, bound together by  $sp^2$  bonds in a honeycomb-style lattice pattern.<sup>1</sup> Since it was first isolated and reported by Geim and co-workers in 2004,<sup>2</sup> graphene has attracted great attention due to its substantial fundamental interest and applied significance in many fields.<sup>3-5</sup> Six years after they published this important discovery, Geim and Novoselov were awarded the Nobel Prize in Physics.

In terms of fundamental research, graphene provides an ideal two-dimensional model system for theoretical studies.<sup>6</sup> With respect to many of its applications, and as with other carbon electromaterials, it is important that graphene is highly conductive. It also has excellent mechanical strength and an unusually large surface area to mass ratio, which makes it a practically useful electromaterial.<sup>1, 3-5</sup> In comparison with amorphous carbon, which is widely used commercially as a support for catalyst immobilization, graphene is far more conductive due to its highly ordered structure.<sup>3</sup> Furthermore, as a nanostructured material, it has an extremely high theoretical surface area to mass ratio of  $2,600 \text{ m}^2 \text{ g}^{-1}$ , even higher than that of single walled carbon nanotube where the inner surface is not readily accessible for many molecules.<sup>7</sup> In contrast with carbon nanotubes, graphene can be generated economically and conveniently using a variety of methods.<sup>8</sup> These properties make graphene an ideal electrocatalyst support in sensing, and energy conversion and storage applications.<sup>9-</sup><sup>12</sup> In terms of electrocatalysis, which is the key focus of this paper, it has been suggested that catalyst activity is significantly improved when graphene is used as the support due to excellent electronic communication achieved between the catalyst and the graphene support in addition to other synergistic effects.<sup>13-17</sup>

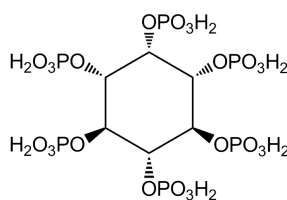
Of particular relevance to the topic under investigation in this paper, a recent study by Liang et al<sup>13</sup> suggested that graphene supported  $\text{Co}_3\text{O}_4$  is a highly efficient and stable catalyst

for both oxygen reduction and oxygen evolution in basic aqueous media. The preparation of this graphene supported  $\text{Co}_3\text{O}_4$  catalyst was simple and involves two steps. In the first, aqueous cobalt acetate solution is added into a GO/ethanol dispersion at room temperature, with stirring for 10 h at  $80^\circ\text{C}$  to generate graphene oxide supported  $\text{Co}_3\text{O}_4$ . In the second step, the reaction mixture provided from the first step is transferred to an autoclave for hydrothermal treatment at  $150^\circ\text{C}$  for 3 h to achieve crystallization of  $\text{Co}_3\text{O}_4$  and reduction of graphene oxide to graphene. Graphene also has been synthesized using wet chemical methods, mechanical exfoliation, chemical vapour deposition,<sup>18</sup> electrochemical reduction of graphene oxide dispersed in weakly alkaline media,<sup>19-21</sup> solvothermal synthesis and other methods.<sup>22</sup>

Generation of a graphene film on a conductive substrate by direct electrochemical reduction of graphene oxide, especially in terms of electrochemical applications, has the advantage of simplicity and leads to excellent electronic communication between the substrate electrode and graphene. A recent study from these laboratories showed that under hydrodynamic conditions, efficient deposition of graphene on a range of electrochemically important conductive substrates such as glassy carbon, gold, indium tin dioxide and platinum can be achieved.<sup>19</sup> Co-deposition of graphene and metallic nanoparticles forms more complex composite materials that can be used in other applications.<sup>23-25</sup>

In this study, we now demonstrate that direct electrochemical reduction provides a facile method for generation of graphene/cobalt nanocomposite materials from an aqueous medium containing  $1 \text{ mg ml}^{-1}$  graphene oxide,  $0.8 \text{ mM}$  cobalt nitrate and  $0.05 \text{ M}$  phytic acid (pH adjusted to 7 using NaOH) which facilitates efficient oxidation of water in alkaline media. Cobalt is an earth abundant element that shows excellent water oxidation activity.<sup>26-29</sup> As in the pioneering work by Nocera et al. who achieved self-repairing of the  $\text{CoO}_x$  catalyst in the presence of phosphate during catalytic water oxidation,<sup>26, 27</sup> the related phytic acid (or phytate in alkaline media), which contains six phosphate groups (Structure I), was found to

facilitate long term stability. Similar to other highly negatively charged polyanions,<sup>30</sup> phytate is also expected to facilitate the formation of nanostructured materials through an electrostatic stabilization mechanism. Moreover, since the phytate anion contains multiple electrostatic binding sites, cobalt oxide may exhibit high stability even if phytate anions are only adsorbed on the surface of cobalt oxide nanoparticles. Consequently, the morphology of the phytate stabilized cobalt oxide nanoparticles may be retained under catalytic turnover conditions. Therefore, it was thought that the use of the phytate anion as stabilizer could be advantageous as it is unlikely to alter the structure of the active sites of the cobalt oxide water oxidation nanocatalyst.<sup>26, 27</sup> Furthermore, the presence of electrostatically confined phytate will have little effect on the accessibility of water molecules to the cobalt oxide surface by due to the well-known hydrogelation property of phytic acid.<sup>31</sup>



**Structure I.** Structure of phytic acid.

The graphene supported cobalt nanocomposite material has been characterized by electrochemical, Raman spectroscopic and scanning electron microscopic techniques. The efficiency of this catalyst for water oxidation also has been quantified using data obtained from voltammetry at a rotating ring disc electrode. High stability under catalytic turnover conditions was verified by the controlled potential electrolysis method. Finally, for the first time, direct detection of all three processes postulated in other studies to be associated with catalysis:  $3 \text{Co(OH)}_2 + 2 \text{OH}^- \rightleftharpoons \text{Co}_3\text{O}_4 + 4 \text{H}_2\text{O} + 2 \text{e}^-$ ,  $\text{Co}_3\text{O}_4 + \text{OH}^- \rightleftharpoons 3 \text{CoOOH} + \text{e}^-$  and  $\text{CoOOH} + \text{OH}^- \rightleftharpoons \text{CoO}_2 + \text{H}_2\text{O} + \text{e}^-$  has been achieved by using large-amplitude Fourier transformed AC voltammetry under catalytic turnover conditions and taking

advantage of the ability of this method to exhibit higher order AC harmonics that are sensitive to processes involving fast electron transfer, but insensitive to the catalytic currents,<sup>32,33</sup> and devoid of background current.<sup>34</sup>

### **Experimental:**

**Chemicals:** Cobalt nitrate, potassium chloride, phytic acid (all Aldrich) and sodium hydroxide (Merck) were used as received from the manufacturer. Deionized water from a MilliQ-MilliRho purification system (resistivity 18 M  $\Omega$  cm) was used to prepare all aqueous electrolyte solutions.

Graphene oxide (GO) was synthesized from natural graphite (crystalline, 300 mesh, Alfa Aesar) using the method described by Hummers et al.<sup>35</sup>

Indium tin oxide (ITO) coated glass slides (surface resistivity: 8-12  $\Omega$  per sq, Aldrich) and Fluorine-doped Tin Oxide (FTO) coated glass slides (surface resistivity: ~12  $\Omega$  per sq, Aldrich) were treated using a literature method, before being used as electrodes.<sup>36</sup>

**Electrochemical co-deposition of graphene/cobalt nanocomposite material from dissolved graphene oxide and cobalt nitrate.** The electrodeposition of graphene/cobalt nanocomposite material from an aqueous 0.05 M phytic acid solution (pH adjusted to 7 using NaOH) containing 1 mg ml<sup>-1</sup> graphene oxide and 0.8 mM Co(NO<sub>3</sub>)<sub>2</sub> was achieved by applying a constant potential of -1.4 V vs. Ag/AgCl (3 M NaCl) in order to simultaneously reduce graphene oxide and Co<sup>2+</sup>. To enhance the rate of co-deposition, the solution was magnetically stirred. Under these conditions, the electrogenerated graphene aggregates and deposits onto the electrode surface together with the metallic cobalt nanoparticles.

**Electrochemistry.** Voltammograms were acquired at 21  $\pm$  2  $^{\circ}$ C with a CHI 760E electrochemical workstation (CH Instruments, Austin, Texas, USA) using a standard three-

electrode electrochemical cell arrangement. For transient cyclic voltammetry, glassy carbon electrodes (CH Instruments, Austin, Texas, USA), indium tin oxide (ITO) or fluorine doped tin oxide (FTO) or graphene/cobalt nanocomposite modified electrodes were used as working electrodes, together with a Pt wire counter electrode and a Ag/AgCl (3M NaCl) reference electrode (0.210 V vs. SHE).<sup>37</sup> For rotating disk electrode (RDE) and rotating ring disk electrode (RRDE) studies, a Rotating Ring Disk Electrode Rotator (RRDE-3A) (ALS Co., Japan) was connected to the electrochemical workstation. A GC disk (4.0 mm diameter) – Pt ring (5.0 mm ID / 7.0 mm OD, ALS Co., Japan) working electrode was used for RRDE studies, while a GC disk (3.0 mm diameter, ALS Co., Japan) or a Pt disk (3.0 mm diameter, ALS Co., Japan) was used for RDE studies, along with the same reference and counter electrodes employed in the cyclic voltammetry. The collection efficiency of the RRDE was determined using analysis of data derived from a 1.0 mM  $K_3(FeCN)_6$  (0.1 M NaCl) solution and calculated to be 0.42. Large-amplitude Fourier transform ac (FTAC) voltammetric measurements were carried out with home-built apparatus,<sup>38</sup> using an applied sine wave perturbation (amplitude 80 mV and frequency 9.02 Hz), superimposed onto the dc ramp. The total current resulted from this applied potential waveform was then subjected to Fourier transformation to obtain a power spectrum. After selection of the frequency band of interest, inverse Fourier Transformation was used to generate the required dc or ac harmonic components.

The glassy carbon working electrodes used in all experiments were polished with an aqueous 0.3  $\mu\text{m}$   $Al_2O_3$  slurry (Buehler), cleaned, sonicated, rinsed with water, and then dried under nitrogen. The solution was purged with nitrogen for at least 10 min before undertaking voltammetric measurements to completely remove  $O_2$ , and then the electrochemical cell was maintained under a positive pressure of nitrogen at all times.

**Scanning Electron Microscopy (SEM)/Energy-dispersive X-ray spectroscopy (EDX):**

SEM images of the electrodeposited graphene and graphene/cobalt nanocomposite modified FTO glasses were obtained using a JEOL JEM 7001 FEGSEM field-emission SEM instrument equipped with an energy-dispersive X-ray (EDX) spectrometer. EDX analysis was conducted at 10 keV.

**Raman Spectroscopy:** Raman spectra of the electrodeposited graphene and graphene/cobalt nanocomposite, cobalt, graphene oxide and graphite modified FTO were obtained using a Renishaw inVia Raman Microscope. An Innova Ar<sup>+</sup> laser (emitting at 514.5 nm) was used as the light source over the 3200 – 100 cm<sup>-1</sup> range.

**X-Ray Diffraction (XRD) Analysis:** XRD measurements were undertaken with a Bruker AXS X-ray diffraction system operating at a voltage of 40 kV and current of 40 mA with CuK $\alpha$  radiation.

**Results and Discussion:*****Characterization of the electrochemically co-deposited graphene/cobalt nanocomposite.***

Initially, SEM-EDX characterization was undertaken on the graphene/cobalt nanocomposite film deposited onto a FTO slide (Fig. 1). Detection of characteristic carbon and cobalt signals suggested successful co-deposition of graphene and cobalt. The presence of phosphorous from phytate anions was also detected. Since there is no realistic mechanism available for phytate anions to become an integral part of the structure of bulk metallic cobalt nanoparticles, the phytate anions are assumed to be adsorbed on the surface of the cobalt nanoparticles and act as a stabilizer during their formation. SEM images reveal layers of graphene and monodispersed cobalt nanoparticles with diameters of about 50 nm uniformly deposited on the graphene support. It is also clear from the SEM image that the graphene layers are not compact.

XRD data obtained on a graphene/cobalt nanocomposite film deposited on a FTO electrode show the expected peaks from the substrate FTO, but none from either Co metal or cobalt oxide, indicating that the deposited material is amorphous.

A graphene/cobalt nanocomposite film deposited on a GC electrode was characterized voltammetrically in an aqueous 0.50 M KCl electrolyte (neutral pH regime) by cycling the potential over the range of -1.0 V to 0 V at a scan rate of 0.05 V s<sup>-1</sup> under a N<sub>2</sub> atmosphere. In comparison with a bare glassy carbon electrode (Fig. 2a), the graphene/cobalt nanocomposite modified one exhibits a much larger capacitance current. This result implies that the electrodeposited graphene/cobalt nanocomposite film is conductive and is not highly compact, so that solvent/electrolyte can penetrate into the film.<sup>17,19</sup> The large reduction current near -1 V, which was not observed with either a bare glassy carbon electrode or a graphene modified electrode, is attributed to the hydrogen evolution reaction catalysed by metallic cobalt generated in this potential region.

A cyclic voltammogram obtained over the potential range of 0 to + 0.7 V in 0.5M KCl showed a large oxidation process on the initial scan which was absent in the second cycle (Fig. 2b), as expected if the stripping of cobalt metal occurs from the electrode surface. Since background contributions from graphene also occur in the same potential region on the first cycle of potential, voltammetric comparison of cobalt loadings in the presence and absence of graphene is not possible under these conditions. However, loading estimate could be made using data obtained in alkaline media, *vide infra*.

Raman spectroscopy is an ideal method for the characterization of graphene.<sup>39</sup> Raman spectra of graphene/cobalt nanocomposite film electrodeposited onto a FTO electrode were obtained using an excitation wavelength of 514.5 nm. The spectra (Fig. 3) obtained from all locations show both the characteristic G band at ~ 1590 cm<sup>-1</sup>, which is associated with the sp<sup>2</sup> carbon atom vibrations, and the D band located at ~ 1350 cm<sup>-1</sup>, which is related to the

presence of disorder in the  $sp^2$  carbon network. The 2D band at  $\sim 2700\text{ cm}^{-1}$  which corresponds to a second order dispersive Raman mode is clearly observed from locations where the graphene layers are thicker (Fig. S1).<sup>40, 41</sup> These results confirm the formation of graphene. The Raman spectra also show five characteristic Raman peaks for  $\text{Co}_3\text{O}_4$  at 188, 513, 605, 472 and  $667\text{ cm}^{-1}$ , which are associated with  $T_{2g}$ ,  $E_g$  and  $A_{1g}$  symmetries.<sup>42</sup> The presence of  $\text{Co}_3\text{O}_4$  is attributed to the oxidation of the surface of cobalt nanoparticles by oxygen when in contact with air due to the reactive nature of cobalt nanoparticles. The small bands at  $123$  and  $242\text{ cm}^{-1}$  are due to the FTO glass.<sup>43</sup>

***Electrocatalytic oxidation of water using graphene/cobalt nanocomposite film modified electrodes in 1 M NaOH media.*** Graphene/cobalt nanocomposite film modified electrodes were placed in contact with 1 M NaOH aqueous solution to determine their activity and stability for catalytic oxidation of water. Cyclic voltammograms obtained in this highly alkaline solution exhibited a very large water oxidation process at  $+0.8\text{ V}$  (Fig. 4) with a current density of  $0.14\text{ A cm}^{-2}$ , which decreases slightly upon repetitive cycling of potential. Extensive bubble formation is observed at the surface and sides of the electrode when the potential is held at  $+0.8\text{ V}$  (Fig. 5). The small decrease in current on cycling the potential is attributed to blocking of the electrode surface by gas bubbles that remain attached to the electrode surface. The current could be restored to close to its initial value under conditions of both cyclic voltammetry and chronoamperometry, after removing the gas bubbles from the electrode surface by taking the electrode out from the solution, rinsing it with water and placing it back in the 1 M NaOH solution. The onset potential for water oxidation is about  $+0.50\text{ V}$ , which represents an overpotential of about  $0.29\text{ V}$  (the thermodynamic reversible potential for the  $4\text{ OH}^- \rightarrow \text{O}_2 + 2\text{ H}_2\text{O} + 4\text{ e}^-$  half reaction at  $22\text{ }^\circ\text{C}$  and  $1\text{ atm O}_2$  in  $0.1\text{ M KOH}$  is calculated to be  $+0.21\text{ V vs. Ag/AgCl}$ ).<sup>44</sup> The large oxidation peak at  $+0.155\text{ V}$  and

the shoulder at around +0.06 V observed on the initial positive potential direction scan indicate the oxidation of metallic cores of cobalt nanoparticles to  $\text{Co(OH)}_2$  and then to  $\text{Co}_3\text{O}_4$ . The much smaller reduction process observed at +0.085 V on reversing the scan direction (process I) is assigned to the reduction of  $\text{Co}_3\text{O}_4$  to  $\text{Co(OH)}_2$ .<sup>45-47</sup> The oxidation and reduction peak currents remained almost unaltered on second and subsequent cycles of the potential. There is also a barely discernible process (II) at around +0.44 V, that will be discussed below.

The presence of phytate plays a crucial role in the catalytic water oxidation by the graphene/cobalt nanocomposite in strongly alkaline media. If it is absent during the deposition of the graphene/cobalt nanocomposite, the catalytic water oxidation current is smaller and decreases substantially in the second and subsequent cycles of the potential, especially when the concentration of NaOH is lowered to 0.1 M (data not shown). This decay is particularly marked under chronoamperometric conditions (about 40% loss in 1000s, Fig. S2) due to the more extensive consumption of  $\text{OH}^-$  during  $\text{O}_2$  evolution ( $4 \text{ OH}^- \rightarrow \text{O}_2 + 2 \text{ H}_2\text{O} + 4 \text{ e}^-$ ) than under cyclic voltammetric conditions, which leads to a decrease in pH. The  $\text{OH}^-$  consumed chronoamperometrically in 10 s is estimated to decrease the average  $\text{OH}^-$  concentration in the diffusion layer by  $\sim 0.36 \text{ M}$ , based on a current density of  $0.14 \text{ A cm}^{-2}$  (Fig. 4), a diffusion coefficient of  $5.3 \times 10^{-5} \text{ cm}^2 \text{ s}^{-1}$  for the  $\text{OH}^-$  ion<sup>48</sup> used for calculation of the diffusion layer thickness, and a faradaic efficiency of 100% (Details of the calculations are provided in the SI section). In principle, if water oxidation is carried out under hydrodynamic rather than stationary conditions, instability due to the consumption of  $\text{OH}^-$  can be avoided. However, in the case of three-dimensional electrode configuration encountered here which is highly desirable for commercial applications, rapid compensation of  $\text{OH}^-$  consumed at the interface is not possible since the mass transport in a porous three-dimensional electrode is slow. Formation of cobalt phosphate due to the presence of phytate

may stop the dissolution of  $\text{CoO}_x$  catalyst when pH decreases and thus improve its stability under catalytic turnover conditions.

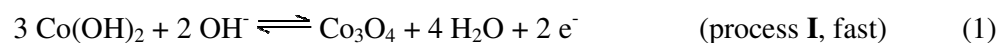
Nocera and co-authors have reported the self-repairing of  $\text{CoO}_x$  catalysts taken place in the presence of phosphate under neutral pH condition. This process helps the re-deposition of  $\text{Co}^{2+}$  formed and released into solution during catalytic water oxidation by formation of stable  $\text{Co}^{3+}$  containing clusters that structurally resemble a molecular cobaltate cluster.<sup>26</sup> In our approach no phosphate needs to be present in the solution during water oxidation, because the phytate anion is co-deposited during graphene/cobalt nanocomposite formation to provide a stabilizing hydrogel monolayer.<sup>31</sup> This proposal is supported by EDX data where phosphorous is detected both before (Fig. 1b) and after (see later, Fig. 10b) water oxidation. In contrast, cyclic voltammograms at a solely graphene modified electrode show only a very small current when the potential is switched at +0.8 V. Furthermore, this current decreases on cycling the potential under the conditions of Fig. 4.

Control experiments also were carried out in the absence of graphene formation but using electrodeposition from an aqueous solution containing the same concentration of  $\text{Co}^{2+}$  and phytic acid (pH 7) and same conditions as for electrodeposition of the graphene/cobalt nanocomposite. Cyclic voltammograms (Fig. S3) at +0.8V in 1 M NaOH now exhibit a current magnitude about 70% that of a graphene/cobalt nanocomposite modified electrode, even though the loading of cobalt is higher (twice that of the graphene/cobalt nanocomposite, as estimated from the area (charge) associated with process I). This confirms that the graphene/cobalt nanocomposite modified electrode provides enhanced catalytic activity. The increase in activity (per cobalt atom) towards water oxidation is presumably due to an increase in the number of active sites of the cobalt catalyst that are in contact with water during catalysis in the presence of the conductive graphene support.

Additional control experiments were carried out to investigate the role of phytate in the electrocatalytic oxidation of water. In this case, a cobalt/graphene modified electrode was deposited in an aqueous solution containing the same amount of graphene oxide and concentration of  $\text{Co}^{2+}$ , but with 0.05 M phosphate buffer (pH 7) instead of phytic acid (pH 7). SEM images obtained under these conditions showed that the Co deposited exhibits a less well-defined nanostructure (Fig. S4a and b) and the EDX spectrum (Fig. S4c) does not reveal the presence of phosphorus. Although the loading of cobalt (estimated from the charge associated with process I) is now about 6 times greater than that of the graphene/cobalt nanocomposite prepared using phytic acid, the current magnitude at +0.8V in 1 M NaOH is only 56% (Fig. S5a). Furthermore, a plot of catalytic current versus time during controlled potential electrolysis at a cobalt – graphene modified GC electrode prepared using phosphate instead of phytate showed a rapid decrease in current to about 2% after 3200s (Fig. S5b). This information confirms the effectiveness of phytate in the formation of the nanostructured cobalt and stabilization of the nanocatalyst under catalytic turnover conditions, presumably via interaction with surface adsorbed phytate and an electrostatic repulsion mechanism.

**FTAC voltammetry.** Dc cyclic voltammograms only provide clear evidence for faradaic oxidative activity in the potential range of 0 to 0.3 V where  $\text{Co}_3\text{O}_4$  containing cobalt in oxidation states II and III is formed. However, higher IV and V valence states of cobalt are believed to be responsible for catalytic water oxidation.<sup>50</sup> Examination of higher order harmonics present under conditions of large-amplitude FTAC voltammetry allows detection of the cobalt reactions that presumably lie underneath the water oxidation process under conditions of dc voltammetry. In FTAC voltammetry, the higher harmonics are devoid of double layer background current which in principle is only present in the dc and fundamental harmonic components, if the double layer capacitance is independent of potential.<sup>34</sup> The

higher order harmonics are also highly sensitive to the electron transfer kinetics of an electrode processes.<sup>51</sup> In particular, ac peak currents decrease dramatically as the rate of the heterogeneous electrode kinetics slows. Consequently, the higher order harmonics are sensitive to fast underlying heterogeneous  $\text{CoO}_x$  electron transfer processes and insensitive to the background water oxidation processes or other catalytic reactions,<sup>32, 33</sup> as applies to dc cyclic voltammetry at higher scan rates.<sup>52</sup> In the present electrode configuration, faradaic currents, devoid of background current, are obtained in the fourth and higher AC harmonic components. Consequently, these higher order harmonic components can be employed to obtain estimations of the reversible potentials of the underlying electron transfer reactions under catalytic turnover conditions. In the FTAC voltammetric method, approximate values of formal reversible potentials can be derived from the average of the valley potentials (potentials of current minimal) available from forward and reverse scans of potential in the case of the even (4<sup>th</sup>, 6<sup>th</sup>, 8<sup>th</sup>, etc.) harmonic components, whereas the average of the peak potentials gives this information in the case of the odd (5<sup>th</sup>, 7<sup>th</sup>, etc.) harmonic components.<sup>53</sup> On this basis, the two major processes (**I** and **III**) have a formal reversible potential of 0.10 and 0.59 V vs. Ag/AgCl, respectively and the minor one (**II**) has a reversible potential of 0.44 V vs. Ag/AgCl (Fig. 6). These reversible potentials, on the basis of the literature reports,<sup>45-47</sup> are associated with the following overall reactions,



However, it should be noted that the formulae given for the cobalt oxides and hydroxides in Eqs 1-3 only indicate the change of oxidation state of cobalt on the voltammetric timescale and provide no structural (phase) information. Furthermore, the combinations of electron

transfer and coupled chemical reactions that contribute to the reversible potentials are unknown.

In FTAC voltammetry, the peak current magnitude directly reflects the electrode kinetics with fast processes giving large currents and slow ones giving smaller currents. Process **II** has a much smaller peak current than processes **I** and **III**, which cannot be solely attributed to the smaller number of electron transferred per cobalt, hence slower kinetics are assumed to apply.<sup>51</sup> Process **III**, which leads to the formation of the active form of the catalyst, is undetectable under dc voltammetric conditions where the major contribution to current in this positive potential region arises from the catalytic water oxidation process. Of course, neither of reactions **I**, **II** or **III** represent just a simple elementary step. Each process represents a combination of hydroxide and electron transfer steps which all influence the potentials detected by FTAC voltammetry. Thus, the values reported of 0.10, 0.44 and 0.59 V are regarded as overall formal potentials.

**Controlled potential electrolysis.** In order to assess the stability of the graphene/cobalt nanocomposite modified electrode under catalytic turnover conditions, constant potential electrolysis experiments were undertaken at an applied potential of 0.8 V vs. Ag/AgCl in 1 M NaOH. During electrolysis, the highly alkaline electrolyte solution was stirred vigorously in an attempt to detach oxygen bubbles adhered to the electrode surface and also to minimize localized pH changes that would otherwise occur during these long timescale experiments. A plot of current density as a function of time up to 30,000s is shown in Fig. 7. Under these conditions, the current decay was small during this prolonged electrolysis experiment. However, even with use of hydrodynamic conditions, complete removal of O<sub>2</sub> bubbles from the electrode surface still was not achieved during electrolysis. In particular, it may be noted that oxygen bubbles remain attached to the electrode surface even 10 minutes after

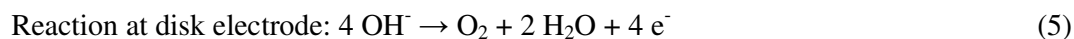
completion of the electrolysis (Fig. 5). Blockage of catalytically active sites by O<sub>2</sub> bubbles is therefore believed to contribute to the slow decay of the current density during the course of long term experiments (30,000 s). This hypothesis is supported by noting that after removal of O<sub>2</sub> bubbles (electrode removed, rinsed with water and re-inserted); the current density is restored back to exactly that found with a freshly modified electrode (Fig. 7).

***Turnover frequency and faradaic efficiency of the graphene/cobalt nanocomposite catalyst calculated from rotating ring disk electrode voltammetric data.***

A rotating ring disk (Pt collection ring for O<sub>2</sub> detection, glassy carbon generation disk) electrode (RRDE), where the glassy carbon disk was modified with graphene/cobalt nanocomposite, was used to quantify the rate of oxygen generation. A Pt RDE electrode was first used to study the mechanism of O<sub>2</sub> reduction in air saturated 1 M NaOH solution, since the nature of oxygen reduction is strongly dependent on the electrolyte and electrode material.<sup>54</sup> Rotation rates over the range 20.9 to 314.2 rad s<sup>-1</sup> were examined. The limiting current is only proportional to the square root of the angular frequency with a zero intercept over rotation rates of 20.9 to 52.4 rad s<sup>-1</sup>, which is the relationship expected if the process is controlled by mass transport. When the rotation rate is above 52.4 rad s<sup>-1</sup>, the positive intercept suggests that the voltammetric process is controlled by both mass transport and kinetics.<sup>55</sup> In order to ensure calibration is undertaken in the mass transport controlled regime, rotation rates of 20.9, 31.4, 41.9 and 52.4 rad s<sup>-1</sup> were used for the estimation of the number of electrons involved in O<sub>2</sub> reduction via use of the Levich equation. A value of 0.25 mM was used for the oxygen concentration in air saturated water.<sup>56</sup> Assuming the diffusion coefficient of oxygen dissolved in 1 M NaOH is  $1.9 \times 10^{-5} \text{ cm}^2 \text{ s}^{-1}$ ,<sup>57</sup> the number of electrons involved in the reduction process was calculated to be  $n = 2 (\pm 0.1)$ . This value is consistent with a literature report obtained in the same medium,<sup>57</sup> and the overall process of oxygen reduction in 1 M NaOH solution at the platinum electrode is assumed to be:



During the RRDE measurements, the disk electrode potential was scanned from 0V to +0.8 V at a rate of 50 mV s<sup>-1</sup>. A constant potential of -300 mV applied to the ring electrode was selected in order to reduce oxygen under mass transport controlled conditions after it was swept to the ring electrode, following generation at the graphene/cobalt nanocomposite modified electrode. The electrode reaction taking place at the GC disk electrode is the following:



while that at the ring electrode is as described in eqn. 4 Fig. 8 shows that O<sub>2</sub> evolution occurs when the potential is more positive than ~0.55 V. In the potential region of 0.5 – 0.8 V, the ring current increases when the disk current increases (more O<sub>2</sub> generated). The oxygen evolution reaction rate in this potential region is controlled by the reactivity of the fully oxidized cobalt oxide complex, since no O<sub>2</sub> was detected in control experiments obtained with a graphene only modified electrode. When cobalt was present, and the rotation rate was varied from 0 to 157.0 rad s<sup>-1</sup>, the voltammetric response at the disk electrode was independent of rotation rate, implying that catalytic water oxidation reaction is kinetically limited. As a consequence, the turnover frequency of the catalyst, *TOF*, defined as the mol of O<sub>2</sub> production/mol of cobalt, can be calculated from the oxygen reduction current at the ring electrode, *I<sub>R</sub>*, using equation (6),<sup>58</sup> where *n* is the number of electrons transferred per oxygen molecule at the ring electrode (*n* = 2), *F* is Faraday's constant, *A* is the area of the disk electrode, *Γ* is the surface concentration of the catalyst, and *N<sub>CL</sub>* is the collection efficiency.

$$TOF = \frac{-I_R}{nFAN_{CL}\Gamma} \quad (6)$$

The surface concentration of cobalt was determined from analysis of the charge associated with the first reduction process at around +0.085 V (inset, Fig. 4). This process remains almost constant during repetitive cycling of potential and thus reflects the quantity of cobalt that is responsible for the oxidation of water. The background corrected charge associated with this process is calculated by integration of the faradaic current vs. potential data and use of the known scan rate to convert the potential base to a time one. The mass of cobalt on the surface is then calculated using Faraday's law. Finally,  $\Gamma$  is calculated using the known geometric area of the glassy carbon disk of the RRDE and eqn. 1 to give a  $\Gamma$  value of  $1.17 \times 10^{-9}$  mol cm<sup>-2</sup>. After substitution into eqn. 6, a  $TOF$  value of 34 s<sup>-1</sup> is obtained at an overpotential of 0.59V. This  $TOF$  value is considered to be a lower limit since the uncompensated resistance is not considered when calculating the overpotential. A faradaic efficiency ( $FE$ ) of 97.7% was calculated based on eqn. 7,<sup>58</sup> where  $n_R = 2$  (2e<sup>-</sup> reduction of O<sub>2</sub> at ring electrode),  $n_D = 4$  (4e<sup>-</sup> O<sub>2</sub> evolution at the disk electrode),  $N_{CL} = 0.42$ .

$$FE = \left| \frac{I_R n_D}{I_D n_R N_{CL}} \right| \quad (7)$$

RRDE voltammograms obtained at a graphene modified electrode showed a small oxidation current at the disk electrode, but close to zero current at the ring electrode, implying that O<sub>2</sub> was not formed at the disk electrode. This confirms that the current detected at the ring electrode when the disk electrode is modified with the graphene/cobalt nanocomposite is indeed due to the reduction of O<sub>2</sub> formed by the oxidation of water catalyzed by cobalt nanoparticles.

In order to further probe the mechanism associated with water oxidation catalyzed by the graphene/Co nanocomposite, a Tafel plot was constructed from the current – potential data. As the current is large, the effect of the uncompensated resistance ( $R_u$ ) of about 18 Ohm is significant. Consequently,  $iR_u$  compensation was employed to obtain the Tafel slope (Fig.

9). The value found of 48 mV/decade is comparable to that of 42 mV/decade reported by Boettcher and co-workers,<sup>29</sup> suggesting that a multi electron transfer process is followed by the rate limiting step.<sup>59</sup> However, the value is considerably smaller than that of 67 mV/decade reported for graphene supported Co<sub>3</sub>O<sub>4</sub> nanocrystals.<sup>13</sup> At an overpotential of 0.3 V (0.51 vs. Ag/AgCl), a *TOF* value of 0.1 s<sup>-1</sup> can be extrapolated from the Tafel plot. This value is considerably larger than those of 0.0032 s<sup>-1</sup> and 4 × 10<sup>-5</sup> s<sup>-1</sup> per cobalt atom for the same overpotential reported previously with a two-dimensional electrode configuration.<sup>29, 60</sup> This result reflects the advantage of using a three dimensional structured electrode in electrocatalysis, since higher accessibility of the active sites to the substrate is achieved.

***Characterization of the graphene/cobalt nanocomposite modified electrode after controlled potential electrolysis.*** SEM images of a graphene/cobalt nanocomposite modified FTO electrode taken after constant potential electrolysis at +0.8 V for 1000s revealed graphene layers with closely and uniformly packed 50 nm particles (Fig. 10a), as expected if the morphology of the nanocatalyst remains unaltered under catalytic turnover conditions. EDX spectra still show the presence of cobalt, carbon, phosphorous and tin (from FTO substrate) with similar intensity levels, along with an increased amount of oxygen (Fig. 10b). These results suggest that the graphene layers and the cobalt particles are stable under the catalytic turnover conditions, and that phytate remains responsible for the stabilization of the nanocatalyst.<sup>26</sup> Interestingly, small holes are observed in some thin graphene layers, but most layers are intact (Fig. S6). These holes are attributed to damage caused by O<sub>2</sub> evolution from underneath the thin graphene layers. This problem may be minimized by using smaller graphene sheets to form electrodes with higher porosity.

Raman spectra obtained from the graphene/cobalt nanocomposite modified FTO slide after controlled potential electrolysis again showed the characteristics D, G and 2D bands of graphene suggesting that graphene is stable under conditions of water oxidation, as well as

five bands at 187, 474, 514, 603 and 669  $\text{cm}^{-1}$  for  $\text{Co}_3\text{O}_4$  (Fig. S7). This and other results confirm that the graphene layers provide a chemically and electrochemically stable support for the cobalt nanocatalyst even under harsh water oxidation – oxygen evolution conditions.

### Conclusions:

A simple and direct electrochemical reduction method has been developed to generate graphene/cobalt nanocomposite materials from a pH 7 aqueous medium containing 1  $\text{mg ml}^{-1}$  graphene oxide, 0.8 mM cobalt nitrate and 0.05 M phytic acid. The highly negatively charged phytate anion was used as a stabilizer for the formation of cobalt nanoparticles. This graphene supported nanocomposite modified electrode allows efficient oxidation of water to oxygen in aqueous 1 M NaOH electrolyte, and has been characterized by electrochemical, Raman spectroscopic and scanning electron microscopic techniques. Phytate ion plays a vital role in achieving high efficiency and stability. A turn over frequency of 34  $\text{s}^{-1}$  at an overpotential of 0.59 V and a faradaic efficiency of 97.7% were measured using rotating ring disk electrode voltammetry. Controlled potential electrolysis data demonstrates that the graphene supported catalyst exhibits excellent stability under harsh catalytic turnover conditions. Large-amplitude Fourier transformed ac voltammetry allowed, for the first time, the direct detection of the electron transfer process that leads to the formation of the active water oxidation catalyst and the determination of reversible potentials.

### Acknowledgement

Financial support from the Australia-India Strategic Research Fund (AISRF) and the Australian Research Council are gratefully acknowledged. The authors also acknowledge technical assistance from the Monash Centre for Electron Microscopy.

**Caption to figures:**

**Fig. 1** SEM image (a) and EDX spectrum (b) obtained from a graphene/cobalt nanocomposite modified FTO glass slide electrode. Deposition of the nanocomposite was undertaken at -1.4 V for 1000 s.

**Fig. 2** (a) Cyclic voltammograms of graphene/cobalt nanocomposite modified GC (—), graphene modified GC (—), cobalt modified GC (—) and bare GC (—) electrodes obtained in 0.5 M KCl at a scan rate of 0.05 V s<sup>-1</sup> over the potential range of -1.0 to 0V. (b) Cyclic voltammograms of graphene/cobalt nanocomposite modified GC electrode in 0.5 M KCl at a scan rate of 0.05 V s<sup>-1</sup> over the potential range of 0 to +0.7 V. Deposition of the nanocomposite at -1.4 V for 1000 s.

**Fig. 3** Raman spectra obtained on a graphene/cobalt nanocomposite modified FTO electrode after deposition at -1.4 V for 1000 s.

**Fig. 4** Electrocatalytic water oxidation by a graphene/cobalt nanocomposite modified glassy carbon electrode (—) in aqueous 1 M NaOH electrolyte at a scan rate of 50 mV s<sup>-1</sup>. The electrode was prepared by deposition of nanocomposite at -1.4 V for 1000 s. Inset shows the cobalt based processes in the potential range of 0 to +0.5 V. The voltammetric response (—) obtained at a graphene modified electrode under the same conditions is provided for comparison.

**Fig. 5** Photograph taken 10 mins after controlled potential electrolysis at 0.8 V with a graphene/cobalt nanocomposite modified electrode in 1 M NaOH. Deposition of nanocomposite at -1.4V for 1000 s.

**Fig. 6.** The third (a), fourth (b) and fifth (c) harmonic components of FTAC cyclic voltammograms obtained from FTAC voltammetry at a graphene/cobalt nanocomposite modified electrode in aqueous 1 M NaOH electrolyte. Dc scan rate = 50 mV s<sup>-1</sup>. Ac amplitude = 80 mV at a frequency of 9.02 Hz. Nanocomposite deposition at -1.4 V for 250 s.

**Fig. 7** Plot of catalytic current versus time during controlled potential electrolysis in 1 M NaOH of a graphene/cobalt nanocomposite modified electrode. Applied potential: 0.8 V vs. Ag/AgCl. Nanocomposite deposition at -1.4 V for 1000 s. (—) 30,000 s electrolysis; (—) additional 6,000s of electrolysis, after gas bubbles generated during initial 30,000s electrolysis period has been removed.

**Fig. 8** RRDE voltammograms obtained for the detection of O<sub>2</sub> generated at the graphene/cobalt nanocomposite modified disk electrode in contact with 1 M NaOH. The potential was scanned from 0 to 0.8V at a rate of 50 mV s<sup>-1</sup> at the disk electrode (—), with a constant potential of -0.3 V being applied to the ring electrode (—). Rotation rate: 52.4 rad s<sup>-1</sup>. Deposition of nanocomposite at -1.4 V for 250 s at a rotation rate of 104.7 rad s<sup>-1</sup>. RRDE voltammograms obtained at a graphene modified electrode under the same conditions are also provided for comparison purpose (disk electrode: —, ring electrode: —).

**Fig. 9** (a) Cyclic voltammogram obtained with  $iR_u$  compensation at a graphene/cobalt nanocomposite modified GC electrode in 1 M NaOH. Scan rate: 50 mV s<sup>-1</sup>,  $R_{comp} = 17.7$

Ohm. Deposition of modified electrode at -1.4 V for 250 s. (b) Tafel plot derived from data in (a). Deposition of nanocomposite at -1.4 V for 1000 s.

**Fig. 10** SEM image (a) and EDX spectrum (b) obtained from a graphene/cobalt nanocomposite modified FTO electrode after controlled potential electrolysis at +0.8 V vs. Ag/AgCl for 1000 s in 1 M NaOH. Deposition of nanocomposite at -1.4 V for 1000 s.

**Notes and references:**

<sup>a</sup> School of Chemistry, Monash University, Clayton, Vic 3800, Australia, E-mails: [alan.bond@monash.edu](mailto:alan.bond@monash.edu), [jie.zhang@monash.edu](mailto:jie.zhang@monash.edu)

<sup>b</sup> Nanoscale Electrocatalysis & Sensor Research Group, Electrodeics and Electrocatalysis Division, CSIR-Central Electrochemical Research Institute, Karaikudi, Tamilnadu, India, E-mail: [klmphani@cecri.res.in](mailto:klmphani@cecri.res.in)

† Electronic Supplementary Information (ESI) available: [Figs. S1–S5, where Fig. S1 contains a Raman spectrum derived from thick graphene layers present on a graphene/cobalt nanocomposite modified FTO electrode, Fig. S2 shows the water oxidation current density as a function of time obtained at a cobalt modified electrode (cobalt deposition in the absence of phytic acid) in 1 M NaOH, Fig. S3 shows the electrocatalytic water oxidation by a cobalt modified electrode (cobalt deposition in the presence of phytic acid) in aqueous 1 M NaOH electrolyte, Fig. S4 shows SEM images and EDX spectrum obtained from a cobalt – graphene modified FTO electrode (prepared in the absence of phytic acid), Fig. S5 shows a cyclic voltammogram and current density vs. time curve of water oxidation at a cobalt – graphene modified electrode (prepared in the absence of phytic acid) in 1M NaOH, and Figs. S6 and S7 show an SEM image and a Raman spectrum obtained from a graphene/cobalt nanocomposite modified FTO electrode after controlled potential electrolysis in 1 M NaOH, respectively. Details of the estimation of the OH<sup>-</sup> consumption that occurs during water electrolysis.] See DOI: 10.1039/b000000x/.

1. A. K. Geim and K. S. Novoselov, *Nat. Mater.*, 2007, **6**, 183-191.
2. K. S. Novoselov, A. K. Geim, S. V. Morozov, D. Jiang, Y. Zhang, S. V. Dubonos, I. V. Grigorieva and A. A. Firsov, *Science*, 2004, **306**, 666-669.
3. D. A. C. Brownson, D. K. Kampouris and C. E. Banks, *Chem. Soc. Rev.*, 2012, **41**, 6944-6976.
4. M. Pumera, *Chem. Rec.*, 2009, **9**, 211-223.
5. M. Liang and L. Zhi, *J. Mater. Chem.*, 2009, **19**, 5871-5878.
6. K. S. Novoselov, A. K. Geim, S. V. Morozov, D. Jiang, M. I. Katsnelson, I. V. Grigorieva, S. V. Dubonos and A. A. Firsov, *Nature*, 2005, **438**, 197-200.
7. S. Stankovich, D. A. Dikin, G. H. B. Dommett, K. M. Kohlhaas, E. J. Zimney, E. A. Stach, R. D. Piner, S. T. Nguyen and R. S. Ruoff, *Nature*, 2006, **442**, 282-286.
8. S. Guo and S. Dong, *Chem. Soc. Rev.*, 2011, **40**, 2644-2672.
9. D. A. C. Brownson, D. K. Kampouris and C. E. Banks, *J. Power Sources*, 2011, **196**, 4873-4885.
10. D. R. Kauffman and A. Star, *Analyst*, 2010, **135**, 2790-2797.
11. Q. Wan, Y. Liu, Z. Wang, W. Wei, B. Li, J. Zou and N. Yang, *Electrochem. Commun.*, 2013, **29**, 29-32.
12. E. J. Lim, S. M. Choi, M. H. Seo, Y. Kim, S. Lee and W. B. Kim, *Electrochem. Commun.*, 2013, **28**, 100-103.
13. Y. Liang, Y. Li, H. Wang, J. Zhou, J. Wang, T. Regier and H. Dai, *Nat. Mater.*, 2011, **10**, 780-786.
14. E. J. Yoo, T. Okata, T. Akita, M. Kohyama, J. Nakamura and I. Honma, *Nano Lett.*, 2009, **9**, 2255-2259.
15. B. Seger and P. V. Kamat, *J. Phys. Chem. C*, 2009, **113**, 7990-7995.
16. R. Kou, Y. Shao, D. Wang, M. H. Engelhard, J. H. Kwak, J. Wang, V. V. Viswanathan, C. Wang, Y. Lin, Y. Wang, I. A. Aksay and J. Liu, *Electrochem. Commun.*, 2009, **11**, 954-957.
17. J. Zhang, S.-X. Guo, Y. Liu, C. Lee, A. M. Bond, Y. Geletii and C. L. Hill, *Energy & Environmental Science*, 2013.

18. C. N. R. Rao, A. K. Sood, K. S. Subrahmanyam and A. Govindaraj, *Angew. Chem. Int. Ed.*, 2009, **48**, 7752-7777.
19. S.-X. Guo, S.-F. Zhao, A. M. Bond and J. Zhang, *Langmuir*, 2012, **28**, 5275-5285.
20. M. Hilder, B. Winther-Jensen, D. Li, M. Forsyth and D. R. MacFarlane, *PCCP*, 2011, **13**, 9187-9193.
21. L. Chen, Y. Tang, K. Wang, C. Liu and S. Luo, *Electrochem. Commun.*, 2011, **13**, 133-137.
22. M. Choucair, P. Thordarson and J. A. Stride, *Nat. Nanotechnol.*, 2009, **4**, 30-33.
23. M. Hilder, O. Winther-Jensen, B. Winther-Jensen and D. R. MacFarlane, *PCCP*, 2012, **14**, 14034-14040.
24. Y. Jiang, Y. Lu, F. Li, T. Wu, L. Niu and W. Chen, *Electrochem. Commun.*, 2012, **19**, 21-24.
25. J. Wu, D. Zhang, Y. Wang, Y. Wan and B. Hou, *J. Power Sources*, 2012, **198**, 122-126.
26. D. A. Lutterman, Y. Surendranath and D. G. Nocera, *J. Am. Chem. Soc.*, 2009, **131**, 3838-3839.
27. M. W. Kanan, J. Yano, Y. Surendranath, M. Dinca, V. K. Yachandra and D. G. Nocera, *J. Am. Chem. Soc.*, 2010, **132**, 13692-13701.
28. J. B. Gerken, J. G. McAlpin, J. Y. C. Chen, M. L. Rigsby, W. H. Casey, R. D. Britt and S. S. Stahl, *J. Am. Chem. Soc.*, 2011, **133**, 14431-14442.
29. L. Trotochaud, J. K. Ranney, K. N. Williams and S. W. Boettcher, *J. Am. Chem. Soc.*, 2012, **134**, 17253-17261.
30. J. Zhang, B. P. Ting, Y. T. Koh and J. Y. Ying, *Chem. Mater.*, 2011, **23**, 4688-4693.
31. L. Pan, G. Yu, D. Zhai, H. R. Lee, W. Zhao, N. Liu, H. Wang, B. C.-K. Tee, Y. Shi, Y. Cui and Z. Bao, *Proceedings of the National Academy of Sciences*, 2012, **109**, 9287-9292.
32. J. Zhang and A. M. Bond, *J. Electroanal. Chem.*, 2007, **600**, 23-34.
33. B. D. Fleming, J. Zhang, A. M. Bond, S. G. Bell and L. L. Wong, *Anal. Chem.*, 2005, **77**, 3502-3510.
34. S. X. Guo, J. Zhang, D. M. Elton and A. M. Bond, *Anal. Chem.*, 2004, **76**, 166-177.
35. W. S. Hummers and R. E. Offeman, *J. Am. Chem. Soc.*, 1958, **80**, 1339-1339.
36. J. Zhang, D. P. Burt, A. L. Whitworth, D. Mandler and P. R. Unwin, *PCCP*, 2009, **11**, 3490-3496.
37. D. T. Sawyer, A. Sobkowiak and J. Roberts, J.L., *Electrochemistry for Chemists*, Wiley, New York, 1995.
38. A. M. Bond, N. W. Duffy, S. X. Guo, J. Zhang and D. Elton, *Anal. Chem.*, 2005, **77**, 186A-195A.
39. C. N. R. Rao, A. K. Sood, K. S. Subrahmanyam and A. Govindaraj, *Angewandte Chemie-International Edition*, 2009, **48**, 7752-7777.
40. Y. Zhu, S. Murali, W. Cai, X. Li, J. W. Suk, J. R. Potts and R. S. Ruoff, *Adv. Mater.*, 2010, **22**, 3906-3924.
41. G. K. Ramesha and S. Sampath, *J. Phys. Chem. C*, 2009, **113**, 7985-7989.
42. D. Gallant, M. Pezolet and S. Simard, *J. Phys. Chem. B*, 2006, **110**, 6871-6880.
43. K. B. R. Kumar, P., *Rec. Res. Sci. Tech.*, 2011, **3**, 48-52.
44. S.-X. Guo, Y. Liu, C.-Y. Lee, A. M. Bond, J. Zhang, Y. V. Geletii and C. L. Hill, *Energy Environ. Sci.*, 2013, **6**, 2654-2663.
45. M. Pontinha, S. Faty, M. G. Walls, M. G. S. Ferreira and M. D. C. Belo, *Corros. Sci.*, 2006, **48**, 2971-2986.
46. M. Pourbaix, *Atlas of electrochemical equilibria in aqueous solutions*, National Association of Corrosion Engineers, 1974.
47. I. G. Casella and M. Gatta, *J. Electroanal. Chem.*, 2002, **534**, 31-38.
48. E. Samson, J. Marchand and K. A. Snyder, *Mater. Struct.*, 2003, **36**, 156-165.
49. J. Zhang and P. R. Unwin, *J. Am. Chem. Soc.*, 2002, **124**, 2379-2383.
50. J. G. McAlpin, Y. Surendranath, M. Dinca, T. A. Stich, S. A. Stoian, W. H. Casey, D. G. Nocera and R. D. Britt, *J. Am. Chem. Soc.*, 2010, **132**, 6882-+.
51. J. Zhang, S. X. Guo, A. M. Bond and F. Marken, *Anal. Chem.*, 2004, **76**, 3619-3629.
52. A. J. Bard and L. R. Faulkner, *Electrochemical Methods: Fundamental and Applications*, Wiley, New York, 2001.

53. K. Bano, A. Nafady, J. Zhang and A. M. Bond, *J. Phys. Chem. C*, 2011, **115**, 24153-24163.
54. J. Zhang, *PEM fuel cell electrocatalysts and catalyst layers: fundamentals and applications*, Springer, 2008.
55. S. Treimer, A. Tang and D. C. Johnson, *Electroanalysis*, 2002, **14**, 165-171.
56. C. Chan, M. Lehmann, K. Chan, P. Chan, C. Chan, B. Gruendig, G. Kunze and R. Renneberg, *Biosens. Bioelectron.*, 2000, **15**, 343-353.
57. C. Zhang, F.-R. F. Fan and A. J. Bard, *J. Am. Chem. Soc.*, 2009, **131**, 177-181.
58. Y. Liu, S.-X. Guo, A. M. Bond, J. Zhang and S. Du, *Electrochim. Acta*, 2013, **101**, 201-208.
59. C. Costentin, S. Drouet, M. Robert and J. M. Saveant, *J. Am. Chem. Soc.*, 2012, **134**, 11235-11242.
60. Y. Surendranath, M. W. Kanan and D. G. Nocera, *J. Am. Chem. Soc.*, 2010, **132**, 16501-16509.